BRAIN COMMUNICATIONS

^{18}F-fluorodeoxyglucose positron emission tomography in dementia with Lewy bodies

Jonathan Graff-Radford,[1] Timothy G. Lesnick,[2,3] Rodolfo Savica,[1] Qin Chen,[4,5] Tanis J. Ferman,[6] Scott A. Przybelski,[2,3] David T. Jones,[1] Matthew L. Senjem,[5] Jeffrey L. Gunter,[5] Walter K. Kremers,[2,3] Clifford R. Jack Jr,[5] Val J. Lowe,[5] Ronald C. Petersen,[1] David S. Knopman,[1] Bradley F. Boeve,[1] Melissa E. Murray,[7] Dennis W. Dickson[7] and Kejal Kantarci[5]

Among individuals with dementia with Lewy bodies, pathologic correlates of clinical course include the presence and extent of coexisting Alzheimer's pathology and the presence of transitional or diffuse Lewy body disease. The objectives of this study are to determine (i) whether ^{18}F-fluorodeoxyglucose PET signature patterns of dementia with Lewy bodies are associated with the extent of coexisting Alzheimer's pathology and the presence of transitional or diffuse Lewy body disease and (ii) whether these ^{18}F-fluorodeoxyglucose pattern(s) are associated with clinical course in dementia with Lewy bodies. Two groups of participants were included: a pathology-confirmed subset with Lewy body disease ($n = 34$) and a clinically diagnosed group of dementia with Lewy bodies ($n = 87$). A subset of the clinically diagnosed group was followed longitudinally ($n = 51$). We evaluated whether ^{18}F-fluorodeoxyglucose PET features of dementia with Lewy bodies (higher cingulate island sign ratio and greater occipital hypometabolism) varied by Lewy body disease subtype (transitional versus diffuse) and Braak neurofibrillary tangle stage. We investigated whether the PET features were associated with the clinical trajectories by performing regression models predicting Clinical Dementia Rating Scale Sum of Boxes. Among autopsied participants, there was no difference in cingulate island sign or occipital hypometabolism by Lewy body disease type, but those with a lower Braak tangle stage had a higher cingulate island sign ratio compared to those with a higher Braak tangle stage. Among the clinically diagnosed dementia with Lewy bodies participants, a higher cingulate island ratio was associated with better cognitive scores at baseline and longitudinally. A higher ^{18}F-fluorodeoxyglucose PET cingulate island sign ratio was associated with lower Braak tangle stage at autopsy, predicted a better clinical trajectory in dementia with Lewy body patients and may allow for improved prognostication of the clinical course in this disease.

1 Department of Neurology, Mayo Clinic, 200 First Street SW, Rochester, MN 55905, USA
2 Division of Biostatistics, Department of Health Sciences Research, Mayo Clinic, 200 First Street SW, Rochester, MN 55905, USA
3 Division of Biomedical Statistics and Informatics, Department of Health Sciences Research, Mayo Clinic, 200 First Street SW, Rochester, MN 55905, USA
4 Department of Neurology, West China Hospital of Sichuan University, Chengdu, China
5 Department of Radiology, Mayo Clinic, 200 First Street SW, Rochester, MN 55905, USA
6 Department of Psychiatry and Psychology, Mayo Clinic, 4500 San Pablo Rd S, Jacksonville, FL 32224, USA
7 Department of Pathology and Laboratory Medicine, Mayo Clinic, 4500 San Pablo Rd S, Jacksonville, FL 32224, USA

Correspondence to: Jonathan Graff-Radford, MD, Department of Neurology, Mayo Clinic, 200 First Street SW, Rochester, MN 55905, USA
E-mail: graff-radford.jonathan@mayo.edu

Keywords: dementia with Lewy bodies (DLB); Lewy body disease (LBD); 18F-fluorodeoxyglucose (18F-FDG); cingulate island sign (CIS); Braak neurofibrillary tangle (NFT)

Received January 3, 2020. Revised February 19, 2020. Accepted March 12, 2020. Advance Access publication April 8, 2020

Abbreviations: 18F-FDG = 18F-fluorodeoxyglucose; CDR-SB = Clinical Dementia Rating Scale Sum of Boxes; CIS = cingulate island sign; DLB = dementia with Lewy bodies; LBD = Lewy body disease; NFT = neurofibrillary tangle

Graphical Abstract

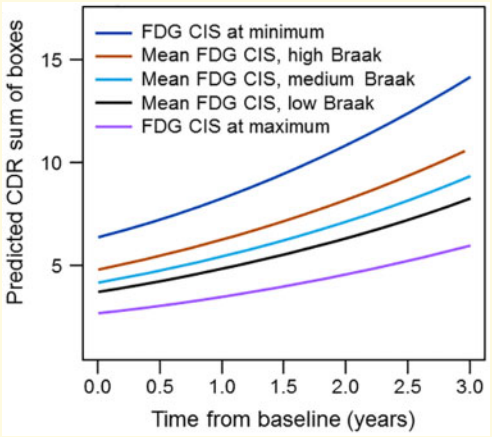

Introduction

The clinical course of probable dementia with Lewy bodies (DLBs) is influenced by the amount of concomitant Alzheimer's neurofibrillary tangle (NFT) pathology, subtype of Lewy body disease (LBD), transitional versus diffuse and burden of α-synuclein pathology (Graff-Radford *et al.*, 2017; Irwin *et al.*, 2017; Ferman *et al.*, 2018). DLB patients have a more aggressive clinical course than Alzheimer's patients, with a shorter survival from disease onset, faster cognitive decline and shorter disease duration before nursing-home admission (Olichney *et al.*, 1998; Williams *et al.*, 2006; Rongve *et al.*, 2014). Therefore, antemortem biomarkers of neuropathology may allow for more accurate prognosis. For example, smaller hippocampal volumes as an indirect surrogate of Alzheimer's disease pathology have been associated with shorter survival among DLB patients (Graff-Radford *et al.*, 2016). DLB patients with a CSF profile suggestive of coexisting Alzheimer's disease pathology are more likely to be admitted to a nursing home and have shorter disease duration than DLB patients without evidence of coexisting Alzheimer's disease pathology in CSF.

Using ^{18}F-fluorodeoxyglucose (^{18}F-FDG) PET, occipital hypometabolism and a higher cingulate island sign (CIS) ratio distinguish patients with DLB from Alzheimer's disease dementia (Lim *et al.*, 2009; Kantarci *et al.*, 2012). The objectives of this study were to (i) determine whether these FDG PET signatures of DLB are associated with pathology in autopsy-confirmed DLB and (ii) to determine whether PET features associate with clinical course in clinically probable DLB.

Materials and methods

Participants

For this study we included two participant groups. The first group were participants with pathologically confirmed LBD who underwent antemortem FDG PET ($n = 34$). For this analysis, the FDG-PET closest to death was used. The second group ($n = 87$) included consecutive participants from the Mayo Clinic Alzheimer's Disease Research Center with a clinical diagnosis of probable DLB (McKeith *et al.*, 2017) who underwent ^{18}F-FDG ($n = 87$). A subset of this group was included in the autopsy-confirmed group. For this analysis, the baseline FDG-PET was used.

As part of the Alzheimer's Disease Research Center evaluation, participants routinely undergo neurological examination and neuropsychological testing. The Clinical Dementia Rating Scale Sum of Boxes (CDR-SB) was used to assess the clinical disease severity of these participants (Berg *et al.*, 1988; Morris, 1993).

DLB clinical features

Participants met consensus criteria for probable DLB (McKeith *et al.*, 2017). Clinical DLB features included the following: (i) visual hallucinations were fully formed, occurred more than once and were not attributable to other medical factors; (ii) Parkinsonism severity was assessed using the Unified Parkinson's Disease Rating Scale, and the presence of parkinsonism was judged to be present or absent by the examining neurologist; (iii) diagnosis of probable rapid eye movement sleep behaviour

disorder or REM behaviour disorder was based on a history of recurrent, apparent dream-enactment behaviour (Boeve *et al.*, 2011); and (iv) a score of 3 or 4 on the Mayo Fluctuations Questionnaire, which is necessary for fluctuations to be considered present (AASM, 2005; Ferman *et al.*, 2004).

MRI and FDG-PET acquisitions

MRI examinations were performed at 3-T with an eight-channel phased array coil (GE Healthcare; Waukesha, WI, USA). A three-dimensional high-resolution magnetization-prepared rapid-acquisition gradient echo acquisition with repetition time/echo time/inversion time of 7/3/900 ms, a flip angle of 8° and 1.2 mm (R/L) × 1.0 mm (A/P) × 1.0 mm (S/I) resolution was performed for anatomical segmentation and labelling. PET images were obtained with a LYSO PET/CT scanner (DRX; GE Healthcare) functioning in three-dimensional mode. Attenuation correction was achieved by obtaining a CT image. Patients received FDG [average (range), 540 (366–399) MBq] injections. An 8-min FDG scan was obtained, after a 30-min FDG uptake period. Image acquisition included four 2-min dynamic frames, acquired from 30 to 38 min after injection. FDG-PET image volumes of each patient were co-registered to the patient's own T_1-weighted MRI scan (Tzourio-Mazoyer *et al.*, 2002). ANTs software (Avants *et al.*, 2011) was employed to compute a deformation from the Mayo Clinic Adult Lifespan Template (Schwarz *et al.*, 2017) to each subject's native MRI space, and the resulting deformation was applied to an in-house modified version of the automated anatomical labelling atlas (Tzourio-Mazoyer *et al.*, 2002). Using the resulting subject-specific atlas, FDG-PET uptake values were extracted from each cortical region of interest. Pons was used as an internal reference region of interest for FDG PET normalization to calculate FDG PET scaled uptake value ratio images. The median value in each target cortical (occipital lobe) region of interest was divided by the median value in the pontine region of interest for FDG PET images. The FDG CIS ratio was defined as posterior cingulate divided by the sum of the precuneus plus cuneus FDG uptake ratio (Schwarz *et al.*, 2017).

Neuropathology

Sampling was done according to the Consortium to Establish a Registry for Alzheimer's Disease protocol (Mirra *et al.*, 1991). Braak NFT stage (Braak and Braak, 1991) and neuritic plaques were interpreted using AT8 immunostaining (1:1000; Endogen, Woburn, MA, USA), thioflavin-S microscopy and a modified Bielschowsky silver stain. Alzheimer's disease was diagnosed using NIA-Alzheimer Association recommendations (Hyman *et al.*, 2012). A monoclonal antibody to α-synuclein (LB509) was used to assess distribution of Lewy body pathology, and LBD cases were classified as brainstem, transitional or diffuse, according to criteria of Fourth Consensus Report of the DLB Consortium (McKeith *et al.*, 2017). Neuropathologists were blinded to the FDG PET results. The analysis in this report focused on Braak NFT stage and Lewy body subtype. Transitional LBD included participants with Lewy-body pathology in brainstem and limbic regions, while diffuse LBD included those with Lewy-related pathology in the neocortex in addition to the brainstem and limbic regions.

Statistical analysis

Demographic and clinical characteristics of the participants were summarized using means and standard deviations for numerical variables and counts and percentages for categorical variables.

We conducted statistical analyses to answer three broad questions in a stepwise fashion:

i. 'Are the FDG PET signatures of DLB patients associated with LBD subtype or Braak NFT stage?'

First, we determined whether the CIS ratio or occipital hypometabolism differed between those with transitional LBD versus diffuse LBD or by Braak NFT stage. We compared the LBD groups using t-tests for numerical variables and chi-squared tests for differences in proportions. For the Braak NFT staging analysis, comparisons were done with ANOVA and chi-squared testing. We did not find an association with occipital hypometabolism, so it was excluded from further analyses.

ii. 'Can we develop data-driven cut-points for the CIS ratio using Braak NFT stage?'

Since the FDG CIS ratio was associated with Braak NFT stage, we wanted to divide the data into subgroups using cut-points. We performed a recursive-partitioning tree algorithm on Braak NFT stage to classify our participants into CIS subgroups.

iii. 'Can the CIS ratio predict the clinical severity and projected course of participants clinically diagnosed with probable DLB?'

Associations between clinical course and CIS ratio

We first ran regression models using age at MRI, education, duration of disease and CIS ratio to predict cognition as measured with CDR-SB and mini-mental state examination (MMSE) in 87 participants with baseline PET. CDR-SB was log-transformed to meet regression assumptions. After fitting the full model, we formed a parsimonious model using backwards elimination. The parsimonious model reduced to a simple linear regression of the CIS ratio on the log of CDR-SB. We repeated this approach with MMSE as an outcome. MMSE was transformed by squaring the values to meet regression assumptions. The parsimonious model was again a simple linear regression with CDR-SB as the predictor. We then ran

mixed models using CDR-SB to investigate longitudinal associations in individuals with data from at least two time points ($n = 51$, 143 records). The mixed models used time from baseline, baseline age at MRI, education, duration of disease and FDG CIS ratio to predict longitudinal cognition (CDR-SB). CDR-SB was again log-transformed to meet regression assumptions. A parsimonious model was formed using backwards elimination. We included random subject-specific intercepts and slopes (a likelihood ratio test indicated that the slopes were necessary, $P < 0.001$). We did not run longitudinal models for MMSE due to the smaller available sample size (37 individuals with missing values).

This study was approved by the Mayo Clinic Institutional Review Board, and informed consent for participation was obtained from every participant and/or an appropriate surrogate.

Data availability

Data from the Mayo Clinic Study of Aging, including data from this study, are available upon request.

Results

Pathology cohort

The characteristics of participants with FDG PET and LBD pathology are summarized in Table 1 by LBD subtype and Braak NFT stage. Three distinct groups (Fig. 1) based on the partitioning analysis—low Braak NFT stage (I–II), medium Braak NFT stage (III–IV) and high Braak NFT stage (V–VI) were identified. The mean FDG CIS ratio was 0.98 for the high Braak group, 1.07 for the medium Braak group and 1.15 for the low Braak group; with a box plot showing the individual observations (Fig. 2).

Clinical cohort

The characteristics of participants in the clinical cohort at the time of baseline FDG PET scan are reported in Table 2. A linear regression model using age at MRI, education, duration of disease and CIS was used to predict cognition (CDR-SB) and reported in Table 3. We found that the CIS ratio was (inversely) associated with CDR-SB (coefficient ± standard error) -2.31 ± 0.65, $P = 0.001$. CIS was the single predictor associated with CDR-SB in the parsimonious model after removing non-significant adjustment variables (-2.40 ± 0.61, $P < 0.001$).

The association between FDG CIS ratio and CDR-SB (line from the parsimonious model) is visualized in Fig. 3. The estimated mean CDR-SB was generally lower (i.e. less impaired) with increasing FDG CIS ratio. We

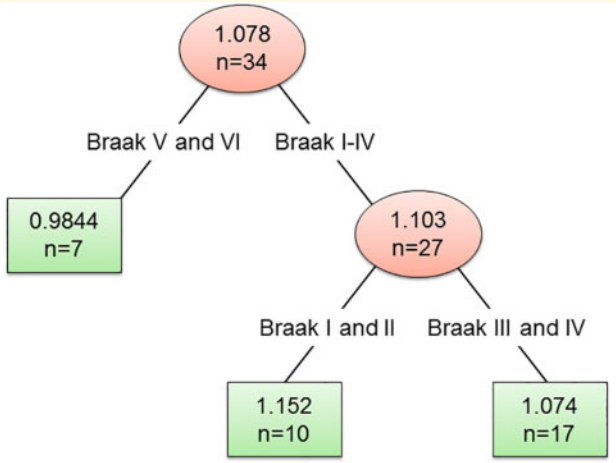

Figure 1 CIS ratio subgroups by Braak NFT stage with recursive partitioning.

Table 1 Characteristics by LBD subtype and Braak NFT stage

	LBD subtype			Braak NFT group			
	DLBD	TLBD	P-value	Low stage I–II	Medium stage III–IV	High stage V–VI	P-value
N	26	8		10	17	7	
Age (years), mean (SD)	72.7 (6.2)	74.6 (9.3)	0.49	72.0 (6.9)	74.3 (7.2)	71.9 (6.9)	0.63
Male, *n* (%)	18 (69)	7 (88)	0.31	10 (100)	12 (71)	3 (43)	0.029
APOE ϵ4 allele, *n* (%)	17 (65.4)	3 (37.5)	0.16	5 (50.0)	8 (47.1)	7 (100.0)	0.045
Years from imaging to death, mean (SD)	2.7 (1.5)	2.1 (1.4)	0.36	2.5 (1.1)	2.3 (1.4)	3.1 (2.0)	0.43
MMSE, mean (SD)	17.3 (6.8)	22.4 (4.4)	0.06	21.3 (5.4)	17.9 (6.3)	16.1 (8.3)	0.26
CDR sum of boxes, mean (SD)	8.3 (4.7)	4.5 (2.2)	0.036	5.0 (3.1)	8.6 (4.7)	8.0 (5.0)	0.12
FDG CIS ratio, mean (SD)	1.07 (0.12)	1.11 (0.09)	0.42	1.15 (0.12)	1.07 (0.07)	0.98 (0.13)	0.008
FDG occipital, SUVR, mean (SD)	1.27 (0.19)	1.34 (0.16)	0.38	1.27 (0.19)	1.28 (0.21)	1.33 (0.10)	0.78
Vis. hallucinations, *n* (%)	16 (67)	4 (67)	1.00	6 (67)	11 (73)	3 (50)	0.59
Fluctuations, *n* (%)	17 (71)	4 (67)	0.84	7 (78)	11 (73)	3 (50)	0.48
Parkinsonism, *n* (%)	17 (71)	6 (100)	0.13	9 (100)	12 (80)	2 (33)	0.010
Probable RBD, *n* (%)	19 (79)	6 (100)	0.22	9 (100)	13 (87)	3 (50)	0.035

CIS = cingulate island sign; DLBD = diffuse Lewy body disease; SD = standard deviation; SUVR = standardized uptake value ratio; TLBD = transitional Lewy body disease.

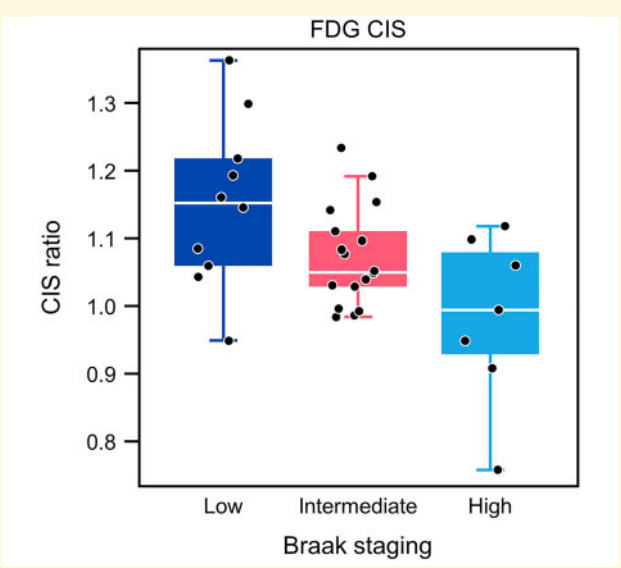

Figure 2 Box plots of CIS ratio by Braak neurofibrillary tangle stage.

Table 2 Demographics of probable DLB participants with baseline FDG PET

	Clinical cross-sectional ($n = 87$)	Clinical longitudinal ($n = 51$)[a]
Age (years), mean (SD)	70.2 (8.0)	70.0 (7.6)
Male, *n* (%)	74 (85)	44 (86)
APOE ϵ4 allele, *n* (%)	36 (46.8)	23 (45.1)
MMSE, mean (SD)	21.2 (6.7)	22.2 (6.3)
CDR sum of boxes, mean (SD)	5.5 (3.4)	4.8 (2.8)
FDG CIS, mean (SD)	1.11 (0.10)	1.12 (0.10)
Visual hallucinations, *n* (%)	52 (59.8)	30 (58.8)
Fluctuations, *n* (%)	61 (70.1)	40 (78.4)
Parkinsonism, *n* (%)	79 (90.8)	47 (92.2)
Probable RBD, *n* (%)	76 (87.4)	46 (90.2)

[a]The clinical longitudinal group is a subset of the cross-sectional group.
RBD = rapid eye movement sleep behaviour disorder.

used the FDG CIS ratios derived from the autopsy cohort (mean FDG).

CIS ratios were 0.98 for the high Braak NFT stage group, 1.07 for the medium Braak NFT stage group and 1.15 for the low Braak NFT stage group to illustrate predicted CDR-SB values at these three important points. The models using MMSE as an outcome showed similar results, with lower FDG CIS ratio associated with greater clinical impairment as measured by MMSE (results not shown).

Longitudinal results

Next, we constructed mixed models on the subset of individuals with at least two time points, using baseline age at MRI, education, duration of disease and CIS ratio to predict longitudinal cognition (CDR-SB) in 51 participants with longitudinal visits (143 observations). CDR-SB was again log transformed to meet regression assumptions. The full and parsimonious models are reported in Table 4. The baseline FDG CIS ratio was associated with log of CDR-SB. There was an interaction between time and disease duration on log CDR-SB indicating the effect of time was less the longer the patient was symptomatic (early in the disease CDR-SB changes more). Using the parsimonious mixed model, predicted values for median education (15 years) and median duration of disease (67 months) were generated. Predicted CDR-SB scores for low values of the FDG CIS ratio (relatively lower posterior cingulate metabolism) start higher (i.e. more impaired) and increase faster than for high values of the FDG CIS ratio. In order to illustrate the possible relationship with pathology, we show predicted values on the plots from the results of the recursive partitioning using the same mean values as before (Fig. 4).

Table 3 Linear regression model predicting CDR-sum of boxes

Predictor	Coefficient (standard error)	*P*-value
Full model ($R^2 = 0.208$)		
Intercept	3.21 (1.02)	0.002
Age	0.002 (0.008)	0.777
Education	0.042 (0.021)	0.047
Duration of disease	0.001 (0.001)	0.516
CIS	−2.31 (0.65)	0.001
Parsimonious model ($R^2 = 0.154$)		
Intercept	4.19 (0.68)	<0.001
CIS	−2.40 (0.61)	<0.001

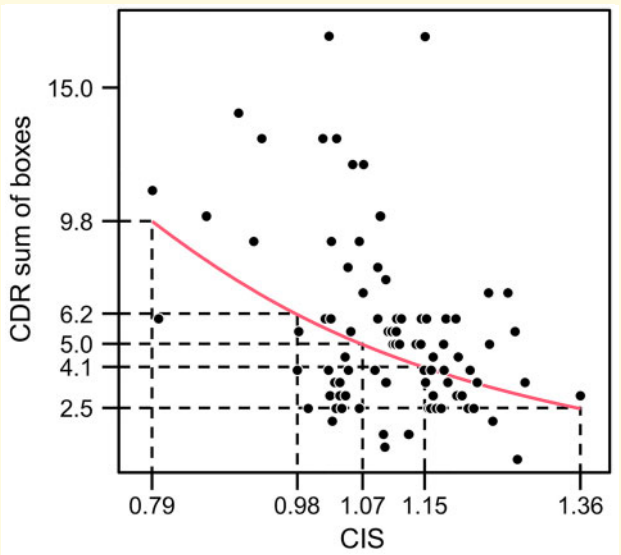

Figure 3 The association between FDG CIS ratio and CDR sum of boxes.

Table 4 Mixed model to predict longitudinal CDR-sum of boxes

Predictor	Coefficient (standard error)	*P*-value
Full model		
Intercept	1.59 (1.09)	0.147
Time	0.14 (0.48)	0.779
Age	0.004 (0.008)	0.618
Education	0.07 (0.02)	0.001
Duration of disease	0.002 (0.001)	0.131
CIS	−1.57 (0.67)	0.023
Time*age	0.003 (0.004)	0.519
Time*education	−0.02 (0.01)	0.092
Time*duration of disease	−0.001 (0.001)	0.053
Time*CIS	0.261 (0.335)	0.437
Parsimonious model		
Intercept	1.93 (0.86)	0.027
Time	0.34 (0.05)	<0.001
Education	0.07 (0.02)	0.001
Duration of disease	0.002 (0.001)	0.127
CIS	−1.55 (0.64)	0.020
Time*duration of disease	−0.001 (0.001)	0.045

*Indicates interaction.

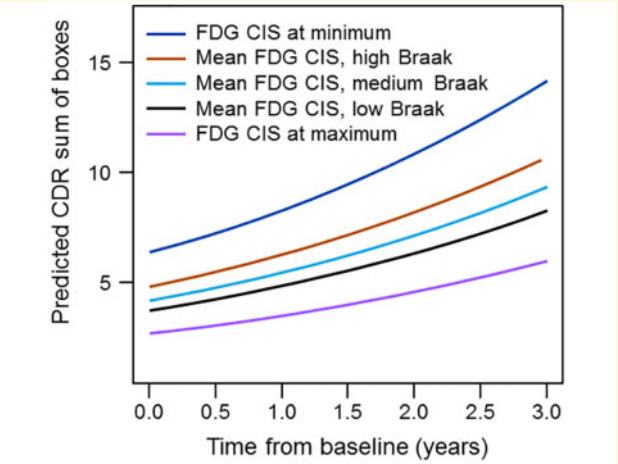

Figure 4 Longitudinal predicted CDR-SB at different CIS ratios reflecting different Braak NFT stages; 'dark blue'—FDG CIS at minimum; 'brown'—mean FDG CIS, high Braak; 'light blue'—mean FDG CIS, medium Braak; black—mean FDG CIS, low Braak; 'violet'—FDG CIS at maximum.

Discussion

The main findings of this study are the following. First, among patients with LBD pathology who underwent antemortem FDG PET, the FDG CIS ratio correlated with Braak NFT stage but not with LBD subtype (transitional LBD versus diffuse LBD). Occipital metabolism was not associated with either Braak NFT stage or LBD subtype. Second, in participants with probable DLB, the FDG CIS ratio was associated with cognition at baseline and longitudinally.

Several studies have highlighted the usefulness of the CIS in distinguishing Alzheimer's dementia from DLB (Lim *et al.*, 2009; Graff-Radford *et al.*, 2014; Imabayashi *et al.*, 2017), but the pathological associations of the CIS have not been clearly delineated. In an earlier study of eight DLB patients, we showed a relationship between higher CIS and lower Braak NFT stage, but only six of these patients had LBD, so confirmation in a larger autopsy series was necessary (Graff-Radford *et al.*, 2014). In contrast, no association with neurodegenerative pathology was found using single-photon emission computed tomography with ^{99m}Tc-hexamethylpropyleneamine oxime in 12 DLB patients (Patterson *et al.*, 2019). However, this imaging technique is known to have lower sensitivity than FDG PET and is a measure of blood flow, not metabolism. In the current larger study, we found a strong relationship between higher (worse) Braak NFT stage and lower (worse) CIS ratio. Similarly, a higher CIS has been associated with less hippocampal atrophy, providing indirect evidence of its association with Alzheimer's disease NFT pathology (Iizuka and Kameyama, 2016). The key finding in our study is that CIS FDG ratios are significantly associated with Braak stage in the DLB spectrum. Additionally, the baseline CIS ratio appears to be a promising biomarker of longitudinal cognitive trajectory in DLB.

Understanding the clinical DLB spectrum requires an appreciation of both Lewy bodies and Alzheimer's disease neuropathology. The majority of patients with DLB who come to autopsy have co-existing Alzheimer's disease pathology (Fujishiro *et al.*, 2008). In a large clinical sample of DLB patients who underwent CSF examination for Alzheimer's disease biomarkers, nearly 40% had biomarker evidence of co-existing Alzheimer's disease (Lemstra *et al.*, 2017). The presence of Alzheimer's disease pathology influences the phenotype and clinical course of LBD patients. For example, burden of NFT was associated with a shorter survival (Irwin *et al.*, 2017) and worse cognitive performance in autopsied LBD patients (Coughlin *et al.*, 2018). Similarly, in patients with a clinical DLB diagnosis, the presence of CSF evidence of co-existing Alzheimer's disease has been associated with a worse cognitive performance and higher risk of nursing home admission (Lemstra *et al.*, 2017). Additionally, DLB patients without hippocampal atrophy on MRI or evidence of amyloid deposition on PET are more likely to respond to acetylcholinesterase inhibitors (Graff-Radford *et al.*, 2012). Therefore, our findings that the CIS ratio predicts clinical progression align with findings from both pathology and biomarker studies.

We did not find a pathological correlate of occipital hypometabolism. It is possible that if we compared Alzheimer's disease dementia cases with DLB cases we would have found a difference, since occipital hypometabolism also distinguishes Alzheimer's disease from DLB (Kantarci *et al.*, 2012).

While the CIS was associated with Braak NFT stage, we did not see a difference in the CIS ratio between transitional and diffuse LBD. Pathological studies have suggested that those with diffuse LBD have a worse prognosis than those with transitional LBD, and when quantified, α-synuclein burden also predicts a worse prognosis (Graff-Radford *et al.*, 2017; Ferman *et al.*, 2018). As both of our FDG measures failed to predict LBD subtype, developing α-synuclein biomarkers is needed to improve the diagnostic capabilities for LB pathology.

Future studies will determine whether direct measures of Alzheimer's disease neuropathology by PET (amyloid and tau) or in the CSF predict the clinical course better than FDG PET. Since a high proportion of DLB patients have concomitant Alzheimer's disease neuropathology, FDG PET may complement the information provided by Alzheimer's disease biomarkers as a diagnostic and prognostic biomarker.

Conclusions

Among pathologically confirmed LBD patients, FDG-PET features varied by Braak NFT stage, but not the LBD subtype. Prior pathology studies and biomarker studies demonstrate that the extent of coexisting NFT pathology of Alzheimer's disease predicts a worse prognosis. The CIS ratio is associated with CDR-SB and MMSE and predicts clinical trajectory in DLB.

Funding

This work was supported by National Center for Research Resources (C06-RR018898); National Institute on Aging (R01-AG050603, P50-AG016574, U01-AG006786, R01-AG011378, R01-AG041851, R01-AG040042); National Institute of Neurological Disorders and Stroke (U01-S100620, R21-NS09468, R01-NS080820); the Mangurian Foundation for Lewy Body Research; the Elsie and Marvin Dekelboum Family Foundation; and the Robert H. and Clarice Smith and Abigail Van Buren Alzheimer's Disease Research Program.

Competing interests

Dr J.G.-R. reports grants from National Institute on Aging. He receives funding from the Alzheimer's Treatment and Research Institute. He received an honorarium from the American Academy of Neurology for serving as a guest editor of Continuum.

Mr T.G.L. reports no disclosures.

Dr R.S. receives research support from the National Institute on Aging, the National Institute of Neurological Disorders and Stroke, the Mayo Clinic Small Grants Program, National Center for Advancing Translational Sciences (NCATS), and an unrestricted grant from Acadia Pharmaceuticals, Inc.

Dr Q.C. reports no disclosures.

Dr T.J.F. receives research support from the National Institute on Aging and the National Institute of Neurological Disorders and Stroke.

Mr S.A.P. reports no disclosures.

Dr D.T.J. receives research support from the National Institute on Aging, the Minnesota Partnership for Biotechnology and Medical Genomics, the National Institute of Biomedical Imaging and Bioengineering and the National Institute on Deafness and Other Communication Disorders.

Mr M.L.S. owns or has owned stocks and/or stock options, in the following medical related companies, unrelated to the current work, within past 3 years: Align Technology, Inc., CRISPR Therapeutics, Gilead Sciences, Inc., Globus Medical Inc., Inovio Biomedical Corp., Ionis Pharmaceuticals, Johnson & Johnson, LHC Group, Inc., Medtronic, Inc., Mesa Laboratories, Inc., Natus Medical Incorporated, Parexel International Corporation, Varex Imaging Corporation.

Dr J.L.G. reports no disclosures.

Dr W.K.K. reports grants from the National Institute on Aging, National Institute of Diabetes and Digestive and Kidney Diseases, National Institute of Neurological Disorders and Stroke, National Institute of Arthritis and Musculoskeletal and Skin Diseases, National Heart, Lung, and Blood Institute, the Juvenile Diabetes Research Foundation and research funding from AstraZeneca, Biogen and Roche.

Dr C.R.J. consults for Eli Lilly and serves on an independent data monitoring board for Roche Holding AG. However, he receives no personal compensation from any commercial entity. He receives research support from the NIA of the NIH and the Alexander Family Professor of Alzheimer's Disease Research, Mayo Clinic.

Dr V.J.L. serves on the scientific advisory boards for Piramal Imaging, Merck Research, INC and Bayer Schering Pharma. He reports receiving funding from the NIH.

Dr R.C.P. is a consultant for Roche Holding AG, Biogen, Merck & Co, Eli Lilly and Co, and Genentech. He receives publishing royalties from Mild Cognitive Impairment (Oxford University Press, 2003) and research support from NIH.

Dr D.S.K. serves on a data safety monitoring board for the Dominantly Inherited Alzheimer Network study. He is an investigator in clinical trials sponsored by Eli Lilly, Biogen, and the Alzheimer's Treatment and Research Institute and receives research support from NIH.

Dr B.F.B. serves as an investigator for clinical trials sponsored by Biogen and Alector. He receives royalties from the publication of a book entitled Behavioral Neurology of Dementia (Cambridge Medicine, 2017). He serves on the Scientific Advisory Board of the Tau Consortium. He receives research support from the NIH,

the Mayo Clinic Dorothy and Harry T. Mangurian Jr. Lewy Body Dementia Program and the Little Family Foundation.

Dr M.E.M. receives research support from the National Institute on Aging, the National Institute of Neurological Disorders and Stroke, the Ed and Ethel Moore Alzheimer's Disease Research Program and the Alzheimer's Association.

Dr D.W.D. receives research support from the National Institute on Aging, the National Institute of Neurological Disorders and Stroke, the State of Florida (Brain Bank), the Michael J. Fox Foundation for Parkinson's Research and AbbVie, Inc.

Dr K.K. serves on the data safety monitoring board for Takeda Global Research & Development Center, Inc.; receives research support from Avid Radiopharmaceuticals, Inc., Eli Lilly and Co. and receives funding from NIH and the Alzheimer's Drug Discovery Foundation.

References

AASM. International Classification of Sleep Disorders, 2nd edn. Diagnostic and Coding Manual. Westchester, IL: American Academy of Sleep Medicine, 2005.

Avants BB, Tustison NJ, Song G, Cook PA, Klein A, Gee JC. A reproducible evaluation of ANTs similarity metric performance in brain image registration. NeuroImage 2011; 54: 2033–44.

Berg L, Miller JP, Storandt M, Duchek J, Morris JC, Rubin EH, et al. Mild senile dementia of the Alzheimer type: 2. Longitudinal assessment. Ann Neurol 1988; 23: 477–84.

Boeve BF, Molano JR, Ferman TJ, Smith GE, Lin SC, Bieniek K, et al. Validation of the Mayo Sleep Questionnaire to screen for REM sleep behavior disorder in an aging and dementia cohort. Sleep Med 2011; 12: 445–53.

Braak H, Braak E. Neuropathological stageing of Alzheimer-related changes. Acta Neuropathol 1991; 82: 239–59.

Coughlin D, Xie SX, Liang M, Williams A, Peterson C, Weintraub D, et al. Cognitive and pathological influences of tau pathology in Lewy body disorders. Ann Neurol 2018; 85: 259–71.

Ferman TJ, Aoki N, Crook JE, Murray ME, Graff-Radford NR, van Gerpen JA, et al. The limbic and neocortical contribution of alpha-synuclein, tau, and amyloid beta to disease duration in dementia with Lewy bodies. Alzheimers Dement 2018; 14: 330–9.

Ferman TJ, Smith GE, Boeve BF, Ivnik RJ, Petersen RC, Knopman D, et al. DLB fluctuations. Specific features that reliably differentiate DLB from AD and normal aging. Neurology 2004; 62: 181–7.

Fujishiro H, Ferman TJ, Boeve BF, Smith GE, Graff-Radford NR, Uitti RJ, et al. Validation of the neuropathologic criteria of the third consortium for dementia with Lewy bodies for prospectively diagnosed cases. J Neuropathol Exp Neurol 2008; 67: 649–56.

Graff-Radford J, Aakre J, Savica R, Boeve B, Kremers WK, Ferman TJ, et al. Duration and pathologic correlates of Lewy body disease. JAMA Neurol 2017; 74: 310–5.

Graff-Radford J, Boeve BF, Pedraza O, Ferman TJ, Przybelski S, Lesnick TG, et al. Imaging and acetylcholinesterase inhibitor response in dementia with Lewy bodies. Brain 2012; 135: 2470–7.

Graff-Radford J, Lesnick TG, Boeve BF, Przybelski SA, Jones DT, Senjem ML, et al. Predicting survival in dementia with Lewy bodies with hippocampal volumetry. Mov Disord 2016; 31: 989–94.

Graff-Radford J, Murray ME, Lowe VJ, Boeve BF, Ferman TJ, Przybelski SA, et al. Dementia with Lewy bodies: basis of cingulate island sign. Neurology 2014; 83: 801–9.

Hyman BT, Phelps CH, Beach TG, Bigio EH, Cairns NJ, Carrillo MC, et al. National Institute on Aging-Alzheimer's Association guidelines for the neuropathologic assessment of Alzheimer's disease. Alzheimers Dement 2012; 8: 1–13.

Iizuka T, Kameyama M. Cingulate island sign on FDG-PET is associated with medial temporal lobe atrophy in dementia with Lewy bodies. Ann Nucl Med 2016; 30: 421–9.

Imabayashi E, Soma T, Sone D, Tsukamoto T, Kimura Y, Sato N, et al. Validation of the cingulate island sign with optimized ratios for discriminating dementia with Lewy bodies from Alzheimer's disease using brain perfusion SPECT. Ann Nucl Med 2017; 31: 536–43.

Irwin DJ, Grossman M, Weintraub D, Hurtig HI, Duda JE, Xie SX, et al. Neuropathological and genetic correlates of survival and dementia onset in synucleinopathies: a retrospective analysis. Lancet Neurol 2017; 16: 55–65.

Kantarci K, Lowe VJ, Boeve BF, Weigand SD, Senjem ML, Przybelski SA, et al. Multimodality imaging characteristics of dementia with Lewy bodies. Neurobiol Aging 2012; 33: 2091–105.

Lemstra AW, de Beer MH, Teunissen CE, Schreuder C, Scheltens P, van der Flier WM, et al. Concomitant AD pathology affects clinical manifestation and survival in dementia with Lewy bodies. J Neurol Neurosurg Psychiatry 2017; 88: 113–8.

Lim SM, Katsifis A, Villemagne VL, Best R, Jones G, Saling M, et al. The 18F-FDG PET cingulate island sign and comparison to 123I-beta-CIT SPECT for diagnosis of dementia with Lewy bodies. Journal of nuclear medicine: official publication. Soc Nucl Med 2009; 50: 1638–45.

McKeith IG, Boeve BF, Dickson DW, Halliday G, Taylor JP, Weintraub D, et al. Diagnosis and management of dementia with Lewy bodies: fourth consensus report of the DLB Consortium. Neurology 2017; 89: 88–100.

Mirra SS, Heyman A, McKeel D, Sumi SM, Crain BJ, Brownlee LM, et al. The Consortium to Establish a Registry for Alzheimer's Disease (CERAD). Part II standardization of the neuropathologic assessment of Alzheimer's disease. Neurology 1991; 41: 479.

Morris JC. The Clinical Dementia Rating (CDR): current version and scoring rules. Neurology 1993; 43: 2412–4.

Olichney JM, Galasko D, Salmon DP, Hofstetter CR, Hansen LA, Katzman R, et al. Cognitive decline is faster in Lewy body variant than in Alzheimer's disease. Neurology 1998; 51: 351–7.

Patterson L, Firbank MJ, Colloby SJ, Attems J, Thomas AJ, Morris CM. Neuropathological changes in dementia with Lewy bodies and the cingulate island sign. J Neuropathol Exp Neurol 2019; 78: 717–24.

Rongve A, Vossius C, Nore S, Testad I, Aarsland D. Time until nursing home admission in people with mild dementia: comparison of dementia with Lewy bodies and Alzheimer's dementia. Int J Geriatr Psychiatry 2014; 29: 392–8.

Schwarz C, Gunter J, Ward C, Vemuri P, Senjem MJ, Wiste H, et al. The mayo clinic adult lifespan template: better quantification across the lifespan. Alzheimers Dement 2017; 13: P792.

Tzourio-Mazoyer N, Landeau B, Papathanassiou D, Crivello F, Etard O, Delcroix N, et al. Automated anatomical labeling of activations in SPM using a macroscopic anatomical parcellation of the MNI MRI single-subject brain. NeuroImage 2002; 15: 273–89.

Williams MM, Xiong C, Morris JC, Galvin JE. Survival and mortality differences between dementia with Lewy bodies vs Alzheimer disease. Neurology 2006; 67: 1935–41.